



## Performance Analysis of Solar Air Heater Having Absorber Plate Artificially Roughened by Chamfered-Square Elements

M. S. Azad<sup>a\*</sup>, A. Layek<sup>b</sup>

<sup>a</sup>CSIR-Central Mechanical Engineering Research Institute, Durgapur, India; \*Email: msazada@gmail.com

<sup>b</sup>Mechanical Engineering Department, National Institute of Technology, Durgapur, India

### ARTICLE INFO

Received: 20 March 2019  
Received in revised form:  
20 April 2019  
Accepted: 25 April 2019  
Available online: 10 May  
2019

### Keywords:

Solar air heater;  
Artificial roughness;  
ANSYS-FLUENT;  
CFD; Overall  
enhancement ratio;  
Thermal performance

### A B S T R A C T

A very common technique to improve the thermo hydraulic performance of solar air heater is providing artificial roughness on absorber plate. Diagonally chamfered cuboids has been used to generate roughness and applied on the absorber surface. A numerical study is performed to study the enhancement of the thermo hydraulic performance of the heater for thoroughness parameters of relative roughness pitch (transverse and longitudinal) of 6 to 14, cross section of cuboids from 8 mm to 14 mm and relative roughness height of 0.44 to 0.088. The Reynolds number is kept in the range of 5000 to 22500 with a constant heat flux of 1000 W/m<sup>2</sup> on the absorber plate. The numerical computation is conducted by using the ANSYS FLUENT CFD software. The standard k-ε turbulence model with enhanced wall treatment has been used to handle the flow turbulence. The Nusselt number and the average friction factor are determined for different values of relative roughness pitch (transverse and longitudinal), cross section of cuboids and relative roughness height. The values of Nusselt number and friction factor of roughened solar air heater is compared with smooth duct at similar flow condition to find out the enhanced performance.

© 2019 Published by University of Tehran Press. All rights reserved.

### 1. Introduction

With rapidly growing population, industrialization, and transportation demand for energy is being continuously rising. The continuous use of limited stock of fossil fuels on the earth, felt energy starvation globally. The uncontrolled use of fossil fuel resulted serious environmental problem, which forced the scientific community to think new and alternate ways to fulfil the future energy demand. The freely and abundantly available solar energy has capability to curb these energy demands among the all sources of renewable energy. The solar insolation gets absorbed by a absorber surface of solar air heater and heat is transferred to the air blowing under it. The hot air gets application in space heating or process heating. The rate of heat transfer between the absorber plate and the blowing air even for the turbulent flow is very low hence

the heat transfer co efficient of a solar air heater (SAH) is very poor. Numerous techniques have so far been used to improve the heat transfer rate and the thermal efficiency of SAH. Some of these are, use of fins [1-4] and packed bed [5], use of artificially roughened absorber plate [6-8] etc. Among these the easiest and the most acceptable method to enhance the thermal performance is the employ of artificially roughened absorber plate for the solar air heater.

The laminar sub-layer is formed on the conventional absorber plate, which is cause of thermal resistance to heat transfer. To destroy the laminar sub-layer, artificial roughness is employed on absorber plate to improve the convective heat transfer by creating turbulence in the flow. This led to increase in friction losses and to overcome from it more power is required by the fan or blower.

Various researchers have investigated the thermo-hydraulic performances of solar air heater embedded with different types of artificial roughness elements with an emphasis on the effect of different roughness parameters. These are comprehensively reviewed by Kumar et al. [8] and not repeated here for the purpose of brevity.

Vyas and Shringi [9] performed CFD based analysis on the solar air heater having baffles as roughness elements to investigate thermal performance and found 2.23 times more heat transfer compared to smooth plates. Vikrant et al. [10] investigated numerically the performance of solar air heater equipped with circular transverse wire ribs as roughness element and found considerable heat transfer enhancement. Prasad and Saini[11] investigated the performance of solar air heater having small diameter wire as roughness element and found considerable enhancement in Nusselt number and friction coefficient at relative roughness pitch of 10. Karwa et al. [12] investigated V-discrete and V-continuous rib as roughness element experimentally and reported that discrete ribs and  $60^\circ$  ribs perform better than the continuous rib and  $45^\circ$  ribs respectively. Rasool et al. [13] ] performed CFD based numerical analysis SAH with double-pass channels having variable rib shapes and found boot shape ribs performing better than house shape and conventional square shape ribs.

It is observed that majority of the works available in the literature except a few are experimental. A numerical analysis can be used successfully as an alternative to the expensive experimental investigation and in quick time several different orientations can be studied for their effectiveness in order to improve the thermal efficiency of SAH. Accordingly, a novel approach is adopted here to use diagonally chamfered cuboid elements to be inserted artificially on the absorber plate of the SAH for making it rough. A numerical

study based on the CFD approach is proposed to investigate the effectiveness of the roughness element for improved thermal performance of the heater.

## 2. Materials and Methods

Diagonally chamfered square elements of 8 mm to 14 mm arm length and 2 to 4 mm height have been used as artificial roughness elements and inserted inner-side of the absorber plate. Various relative roughness pitches (transverse and longitudinal) have been used for investigation. The hydraulic diameter ( $D$ ) of SAH duct used for investigation is 45 mm. A uniform heat flux of  $1000\text{W/m}^2$  has been applied on the absorber plate for entire investigation. Reynolds number ranging from (Re) 5000 to 22500, have been used for study to observe the effect of the roughness on nusselt number and friction factor as the SAH generally operates at the same range.

The detail of the roughness is explained in Fig. 1. Remaining all three sides of test duct are considered as smooth surfaces. A SAH duct having dimensions as 2100mm long(L) , 200mm width(W) and 25 mm height(H) have been used for CFD analysis. The aspect ratio 8 was constant for entire study. The flow domain was divided in three sections i.e., entry section, entry section and test section. To minimise the end effects the entry section (725mm) and exit section (325mm) of the flow domain were kept sufficiently large.

A secondary flow is assume to be happen as the roughness geometry is inclined in the transverse direction of air flow, therefore a 3D flow domain have been selected for the study. ICFM CFD of ANSYS 13.0 is used for meshing of domain in the present work [14]. Finer mesh in the rib region and relatively coarser mesh for other region has been used for accurately examine the flow behaviour and heat transfer.

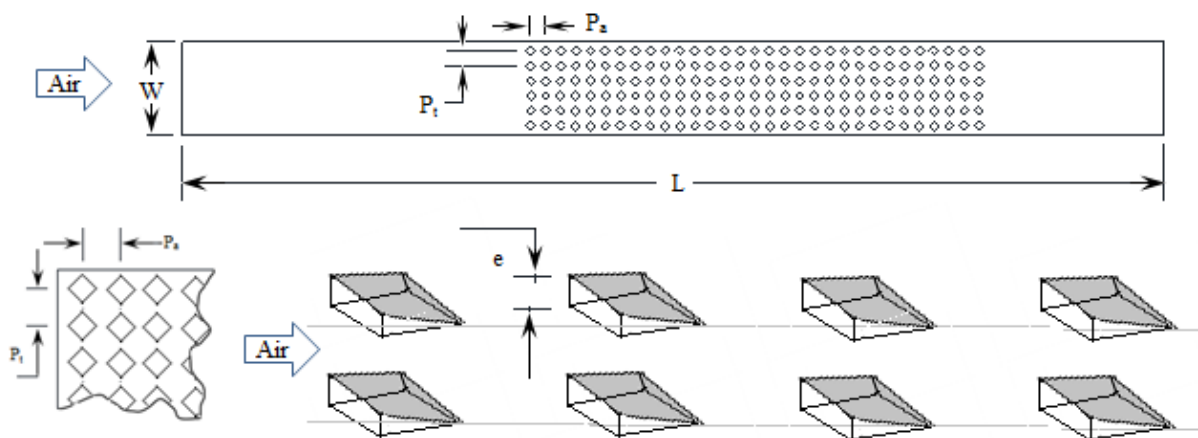


Figure 1. Detailed of the roughness elements

The system of governing equation consists of the continuity, momentum and energy equations. The governing equations for 3-D domain are shown below:

Continuity equation:

$$\frac{\partial u}{\partial x} + \frac{\partial v}{\partial y} + \frac{\partial w}{\partial z} = 0 \quad (1)$$

Momentum equation:

$$u \frac{\partial u}{\partial x} + v \frac{\partial u}{\partial y} + w \frac{\partial u}{\partial z} = -\frac{1}{\rho} \frac{\partial p}{\partial x} + \nu \left( \frac{\partial^2 u}{\partial x^2} + \frac{\partial^2 u}{\partial y^2} + \frac{\partial^2 u}{\partial z^2} \right) \quad (2)$$

$$u \frac{\partial v}{\partial x} + v \frac{\partial v}{\partial y} + w \frac{\partial v}{\partial z} = -\frac{1}{\rho} \frac{\partial p}{\partial y} + \nu \left( \frac{\partial^2 v}{\partial x^2} + \frac{\partial^2 v}{\partial y^2} + \frac{\partial^2 v}{\partial z^2} \right) + g\beta(T - T_\infty) \quad (3)$$

$$u \frac{\partial w}{\partial x} + v \frac{\partial w}{\partial y} + w \frac{\partial w}{\partial z} = -\frac{1}{\rho} \frac{\partial p}{\partial z} + \nu \left( \frac{\partial^2 w}{\partial x^2} + \frac{\partial^2 w}{\partial y^2} + \frac{\partial^2 w}{\partial z^2} \right) \quad (4)$$

Energy equation:

$$u \frac{\partial T}{\partial x} + v \frac{\partial T}{\partial y} + w \frac{\partial T}{\partial z} = \alpha \left( \frac{\partial^2 T}{\partial x^2} + \frac{\partial^2 T}{\partial y^2} + \frac{\partial^2 T}{\partial z^2} \right) \quad (5)$$

where  $u$ ,  $v$ ,  $w$  are the components of the fluid velocity in  $x$ ,  $y$  and  $z$  directions of the rectangular Cartesian coordinate,  $p$  is the pressure,  $T$  is the temperature and  $T_\infty$  is the ambient temperature. The thermo-physical properties are described through the density ( $\rho$ ), kinematic viscosity ( $\nu$ ), thermal diffusivity ( $\alpha = k/\rho C_p$ ) with  $k$  being the thermal conductivity and  $C_p$  the specific heat at constant pressure,  $\beta$  is the volumetric thermal expansion coefficient and  $g$  is the acceleration due to gravity.

In the present study of CFD analysis of SAH duct ANSYS FLUENT 13.0 has been used as computational tool. A 3D model of computational domain has been used due to presence of secondary flow in transverse direction. A fully developed, steady and turbulent flow is assumed. It is also assumed that all walls of duct except

absorber plate are adiabatic and the working fluid air is incompressible for the test range of SAH. These assumptions were made based on the previous investigations done by the researchers in their experiments. Table.1 shows the thermophysical properties of air and aluminum plate which are working fluid and absorber plate respectively.

Parameter	Air	Absorber plate (aluminium)
Specific heat ( $C_p$ , J/kgK)	1004.9	871.00
Thermal conductivity ( $k$ , W/mK)	0.02624	202.40
Density ( $\rho$ , kg/m <sup>3</sup> )	1.225	2719.00
Viscosity ( $\mu$ , N/m <sup>2</sup> )	$1.846 \times 10^{-5}$	-
Thermal expansion coefficient ( $\beta$ , K <sup>-1</sup> )	0.0034	-

The boundary conditions of solution domain were specified as, velocity inlet at inlet and outflow at outlet. The turbulence has been specified by turbulence intensity and hydraulic diameter. The boundary condition applied at absorber plate was constant heat flux. SIMPLE (semi-implicit method for pressure linked equations) algorithm with second order upwind numerical scheme of the governing equations has been used for the pressure-velocity coupling.

### 3. Selection and Validation of Model

It is very essential to choose and validate the best fitted turbulence model for computational analysis. For the smooth duct having same cross section Dittus-Boelter empirical correlation [15] for the Nusselt number and modified Blasius equation for the friction factor have been compared with various turbulence models such as Standard (STD)  $k$ - $\epsilon$  model and Realizable (RLG)  $k$ - $\epsilon$  model.

Dittus-Boelter correlation for smooth duct:

$$Nu = 0.024 Re^{0.8} Pr^{0.4} \quad (6)$$

Modified Blasius equation:

$$f_s = 0.085 Re^{-0.25} \quad (7)$$

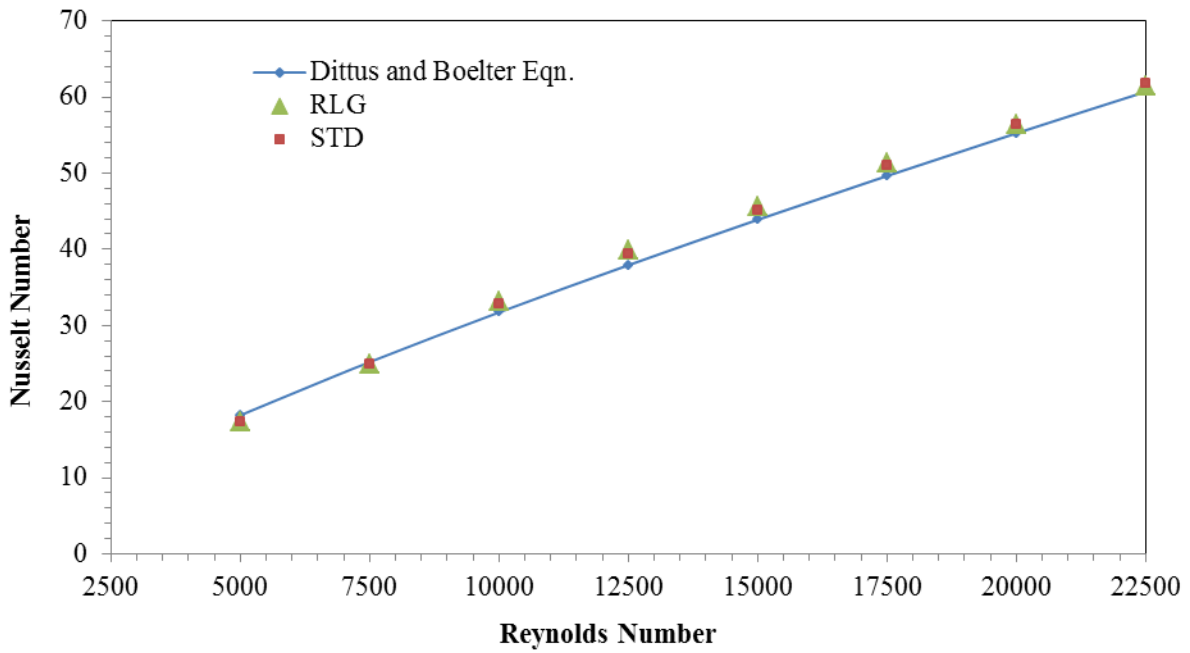


Figure 2. Variation of Nusselt number for different predicted turbulence models with the Dittus-Boelter relation for smooth duct

Amongst the all predicted values the STD  $k-\epsilon$  turbulence model have been found best fitted with the Dittus-Boelter empirical correlation and the modified Blasius equation results. It is very clearly shown in, Fig.2 where Dittus-Boelter correlation results have been compared with various turbulence models for Nusselt number varying with Reynolds number for smooth duct. Similarly it is shown in, Fig.3 for modified Blasius correlation

results which have been compared with various turbulence models for friction factor varying with Reynolds number. The values found for STD  $k-\epsilon$  turbulence model are within 5% deviation from the predicted value from the Dittus-Boelter correlation and modified Blasius equation for the Nusselt number and friction factors respectively are within acceptable limit. Based on the validation results STD  $k-\epsilon$  turbulent model is selected for CFD analysis of SAH duct to get best result.

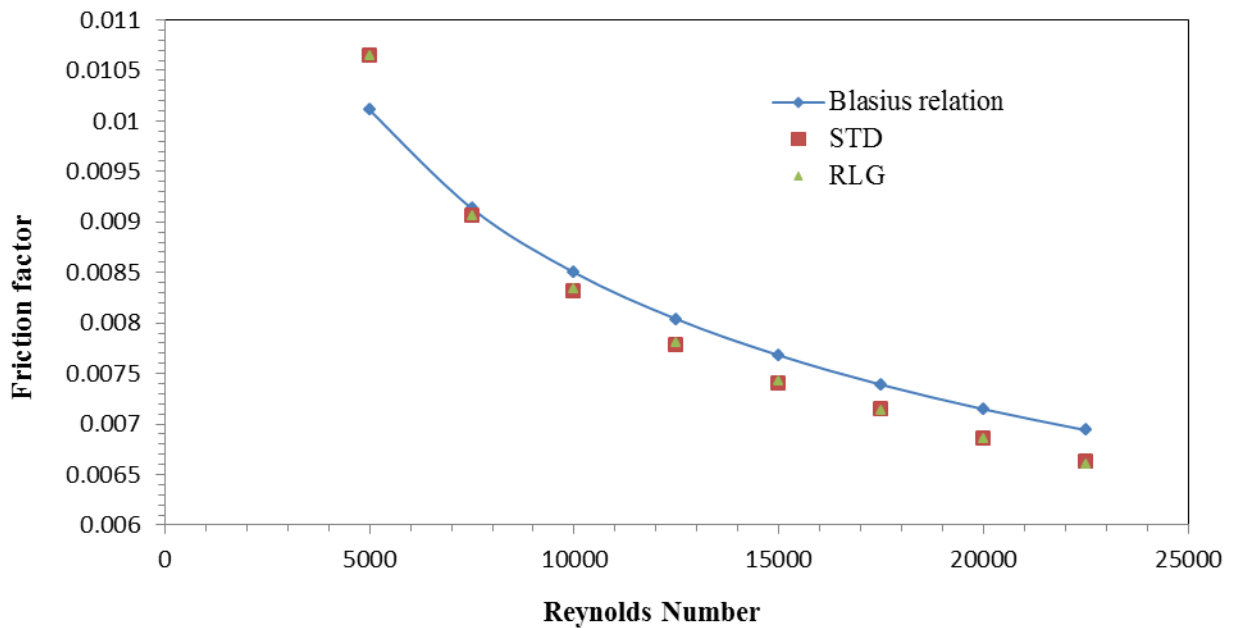


Figure 3. Variation of friction factor for different predicted turbulence models with the modified Blasius relation for smooth duct.

#### 4. Results & Discussion

All simulation results found for the roughened absorber plate are presented and compared with the smooth plate result. The improvement in thermohydraulic performance of the SAH for variable flow rate is discussed below.

##### 4.1. Heat Transfer

Nusselt number is function of heat transfer and shows the thermal behaviour of the SAH. Fig.4, 5 and 6, shows that the Nusselt number is directly dependent on Reynolds number as Nusselt number increases with increase in its Reynolds number for roughened as well as smooth plate. The variation

of Nusselt number with respect to Reynolds number for different relative roughness pitch (longitudinal pitch,  $P_a/e = 6, 7, 8$  and transverse pitch,  $P_t/e = 4, 6, 7, 8$ ), fixed element size and fixed relative roughness height of the roughness element is shown in Fig.4. The variation of Nusselt number with respect to Reynolds number for different element size having fixed longitudinal and transverse relative roughness pitch ( $P_a/e = 7, P_t/e = 7$ ) and fixed Relative roughness height is shown in Fig.5. Similarly, The variation of Nusselt number with respect to Reynolds number for different relative roughness height having fixed element size and fixed longitudinal and transverse relative roughness pitch ( $P_a/e = 6, P_t/e = 6$ ) is shown in Fig. 6.

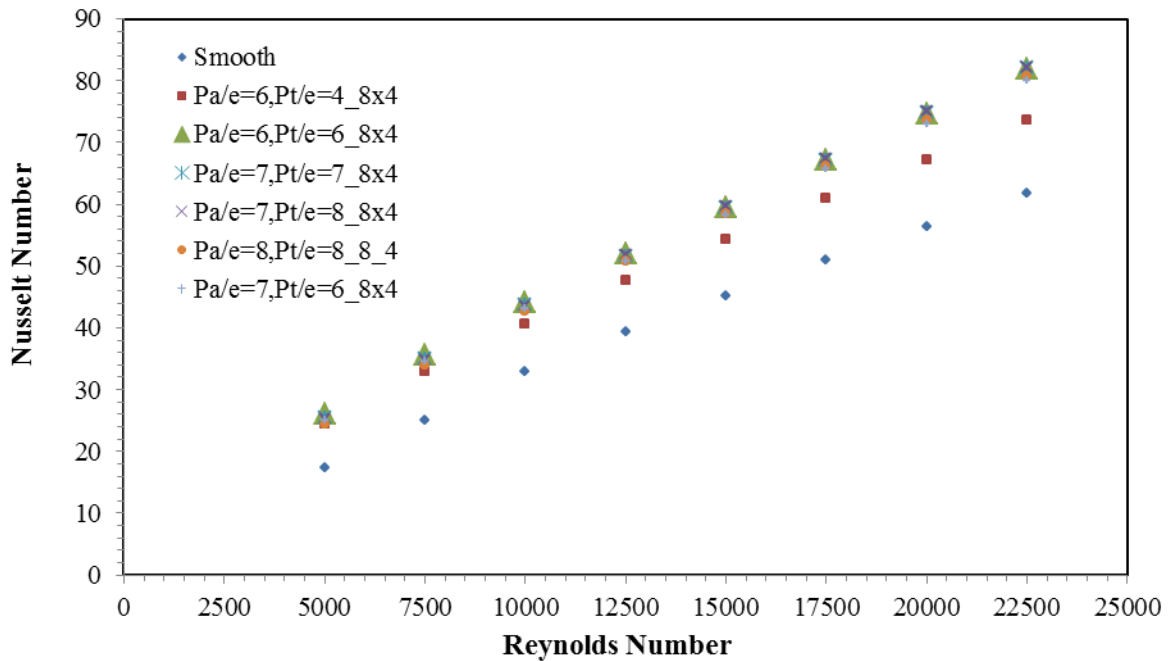


Figure 4. Variation of Nusselt Number for different relative roughness pitches having fixed element size and fixed relative roughness height.

It can be clearly observed from the above plots that increase in the relative roughness pitch, cross sectional area and relative roughness height, increases the value of Nusselt number. It can be also observed that the Nusselt number increases substantially for the roughened plate in comparison to the smooth plate. Hence, the SAH embedded with the artificial roughness element is found to be more effective in a sense that it provides enhanced thermal performance. The highest Nusselt number is found as 84.3 at  $P_a/e = 7, P_t/e = 7$  (with element cross section of  $12 \times 4$ ).

##### 4.2. Friction Factor

Friction factor affects the thermohydraulic performance of SAH. The effect of roughness on friction factor studied is shown in Fig.7, 8 and 9. The variation of friction factor with respect to Reynolds number for different relative roughness pitch (longitudinal pitch,  $P_a/e = 6, 7, 8$  and transverse pitch,  $P_t/e = 4, 6, 7, 8$ ) fixed cross section of the roughness element ( $8 \times 4$ : arm  $\times$  height) and fixed relative roughness height is shown in Fig.7. The variation of friction factor with respect to Reynolds number for different element size having fixed longitudinal and transverse relative roughness pitch ( $P_a/e = 7, P_t/e = 7$ ) and fixed Relative roughness height is shown in Fig.8.

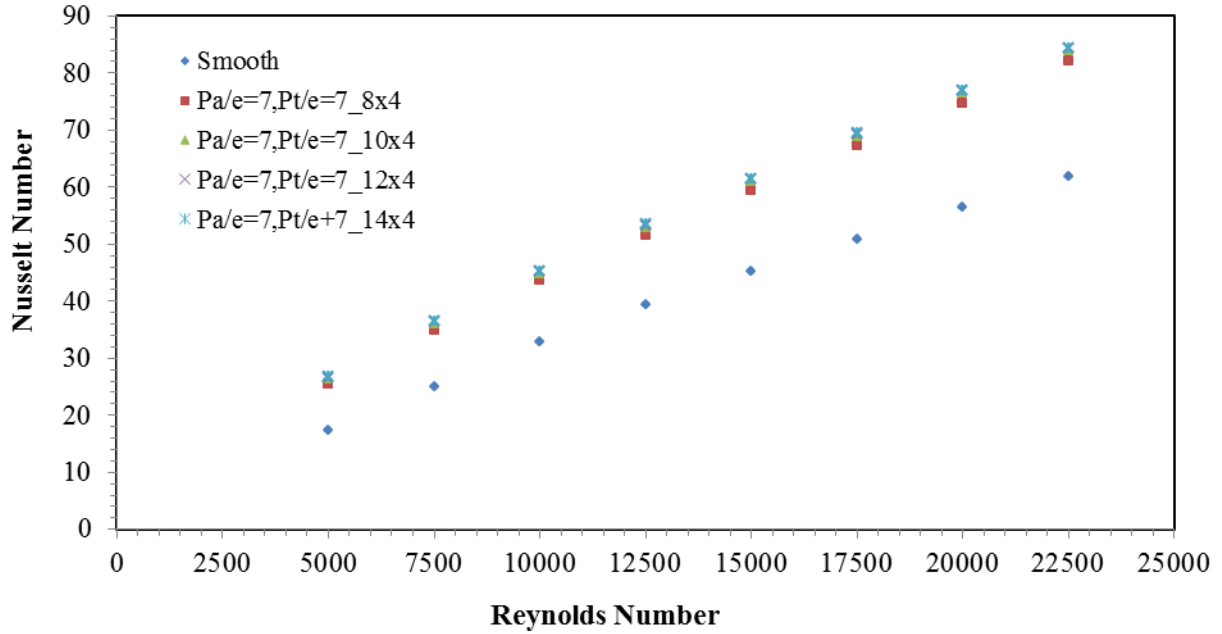


Figure 5. Variation of Nusselt Number for different element size having fixed relative roughness pitch and fixed relative roughness height.

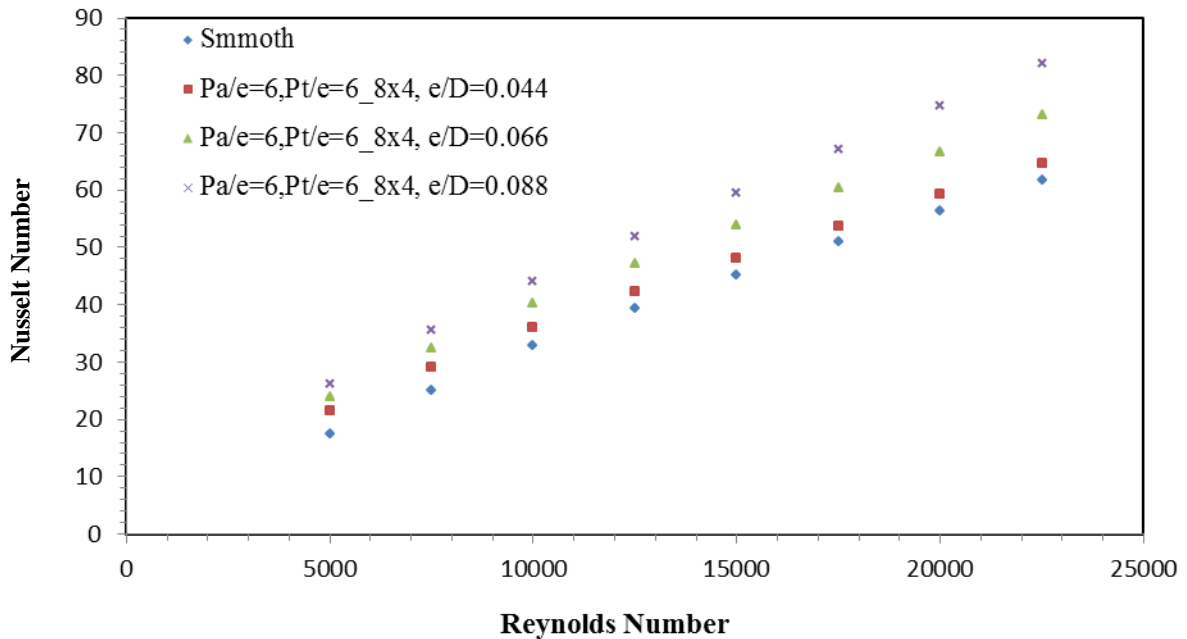


Figure 6. Variation of Nusselt Number for different relative roughness height having fixed element size and fixed relative roughness pitch.

Similarly, The variation of friction factor with respect to Reynolds number for different relative roughness height having fixed element size and fixed longitudinal and transverse relative roughness pitch ( $P_a/e = 6$ ,  $P_t/e = 6$ ) is shown in Fig. 9. It can be clearly observed from the above plots that with increase in Reynolds number the value of the

friction factor decreases. This happens due to the suppression of laminar sub-layer for fully developed turbulent flow in the SAH duct. The maximum and minimum friction factor for the roughened absorber plate found is 0.0149 at  $Re = 5000$  for  $P_a/e = 7$ ,  $P_t/e = 7$  (with cross section  $14 \times 4$ ) and 0.00702 at  $Re = 22,500$  for  $P_a/e = 7$  and  $P_t/e = 7$  (with cross section  $8 \times 2$ ) respectively.

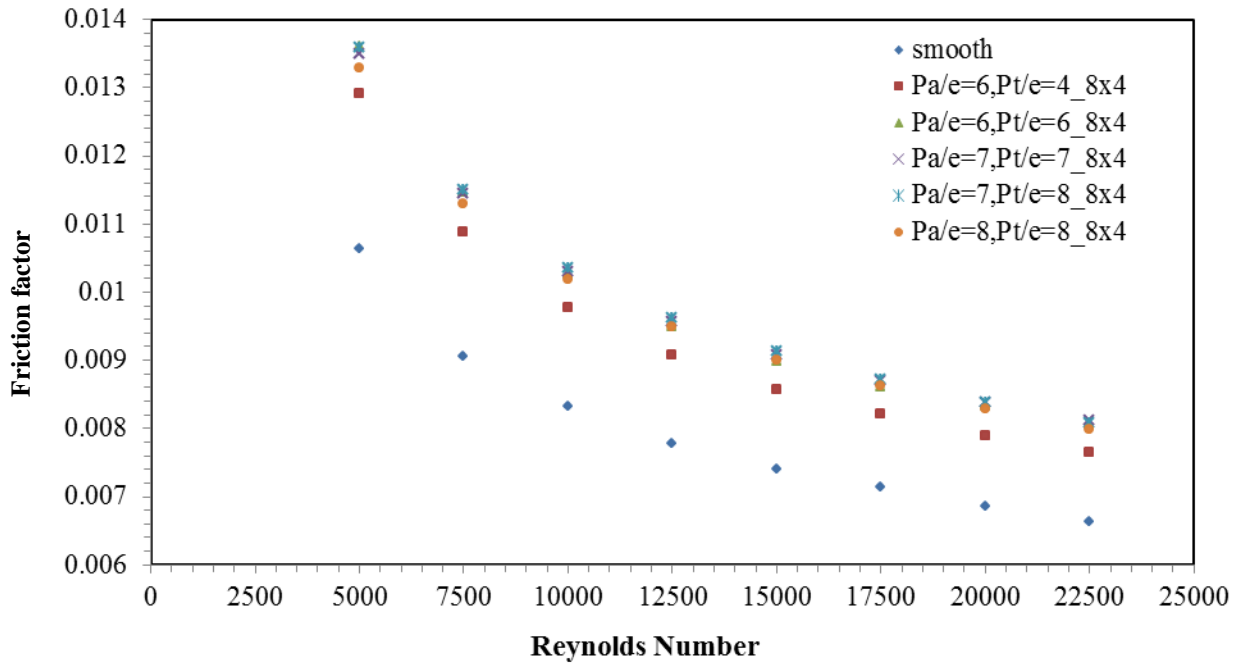


Figure 7. Variation of friction factor for different relative roughness pitch having fixed element size and fixed relative roughness height.

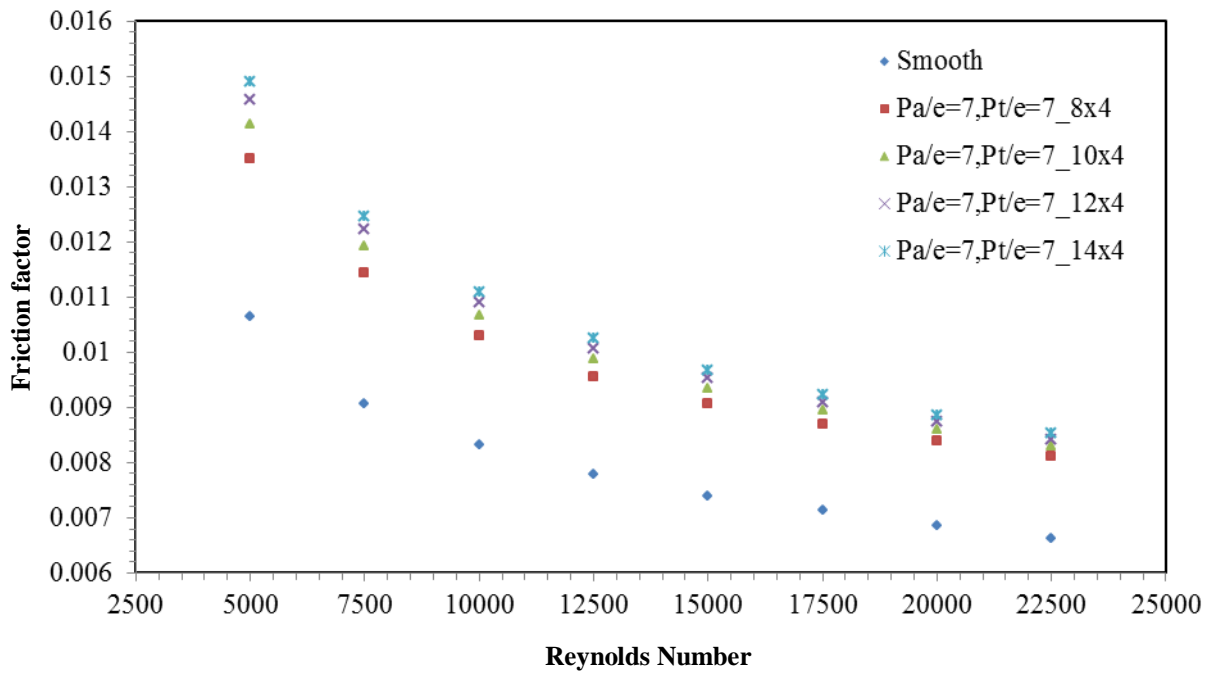


Figure 8. Variation of friction factor for different element size having fixed relative roughness pitch and fixed relative roughness height.

#### 4.2. Nusselt number enhancement ratio

The enhancement ratio of the Nusselt number is defined as the ratio of the Nusselt number obtained

of the roughened absorber plate to that of the smooth absorber plate [13] and can be calculated as;

$$\frac{Nu_r}{Nu_s}$$

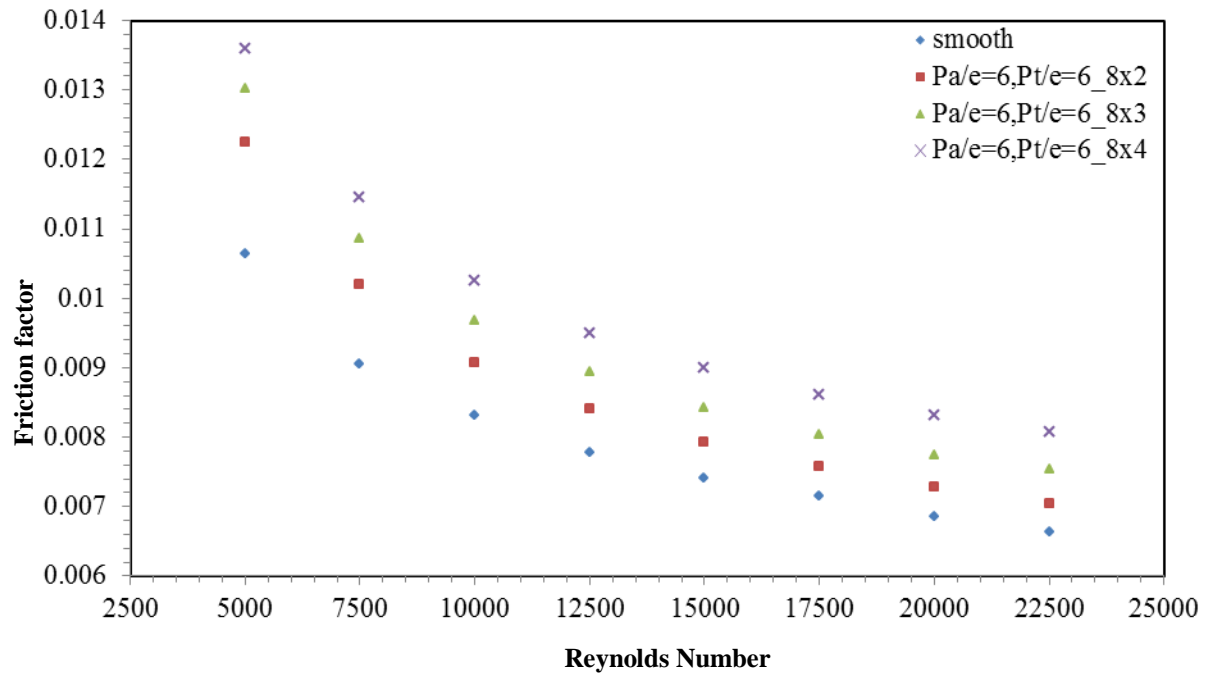


Figure 9. Variation of friction factor for different relative roughness height having fixed element size and fixed relative roughness pitch

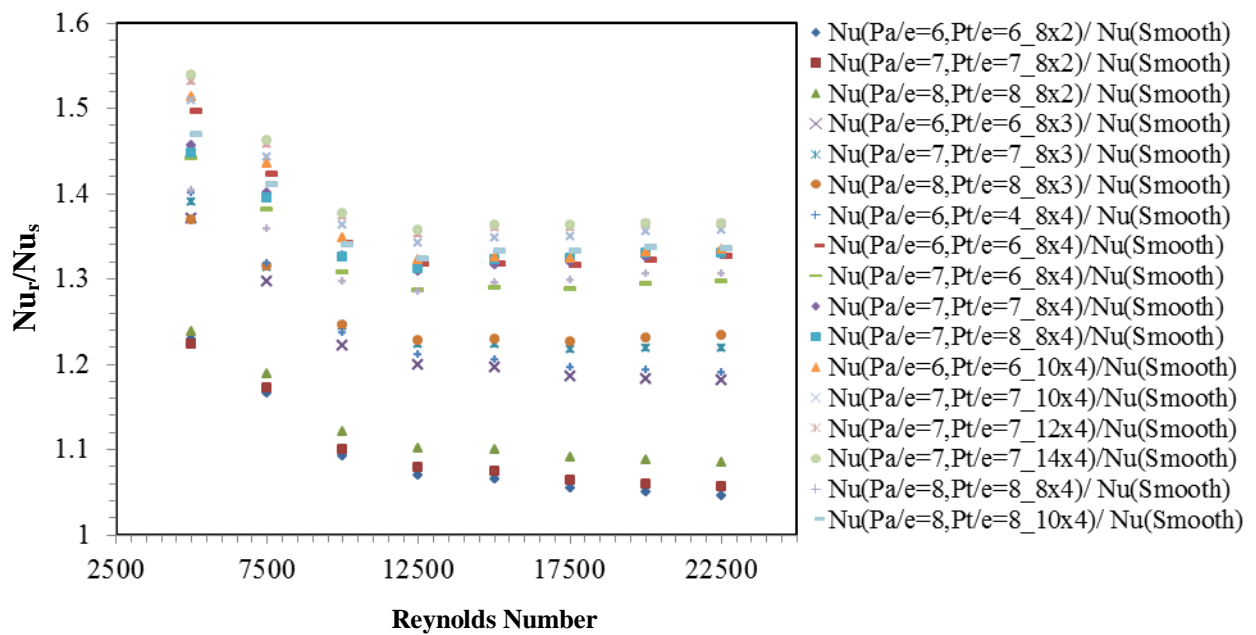


Figure 10. Variation of Enhancement ratio with respect to Reynolds number

Generally the entire configurations give significant enhancement in Nusselt number i.e.  $\frac{Nu_r}{Nu_s} > 1$  for the range of Reynolds number studied. Fig. 10 shows that enhancement ratio is 1.54 at  $P_a/e=7$ ,  $P_t/e=7_{14x4}$ . Using the diagonally cut square element as roughness element an increase on 54% in Nusselt number is found. The maximum value of enhancement ratio of Nusselt number is found at

least Reynolds number. The value of enhancement ratio of Nusselt number decreases with increase in Reynolds number for all sets of configurations considered.

#### 4.3. Friction factor ratio

Similarly, the friction factor ratio is defined as the ratio of the friction factor obtained of the roughened absorber plate to that of the smooth absorber plate [13] and can be calculated as;  $\frac{Fr_r}{Fr_s}$

Similar to the enhancement ratio of the Nusselt number, the friction factor ratio also gives greater value for entire configurations i,  $e \frac{Fr_r}{Fr_s} > 1$  for the range of Reynolds number studied. Fig. 11 shows that highest friction factor ratio is 1.4 at  $P_d/e=7$ ,  $P_t/e=7$ , cross section of 14x4. Using the diagonally

cut square element as roughness element an increase in 40% in friction factor is found.

The maximum value of friction factor ratio is found at least Reynolds number. The value of friction factor ratio decreases with increase in Reynolds number for all sets of configurations studied.

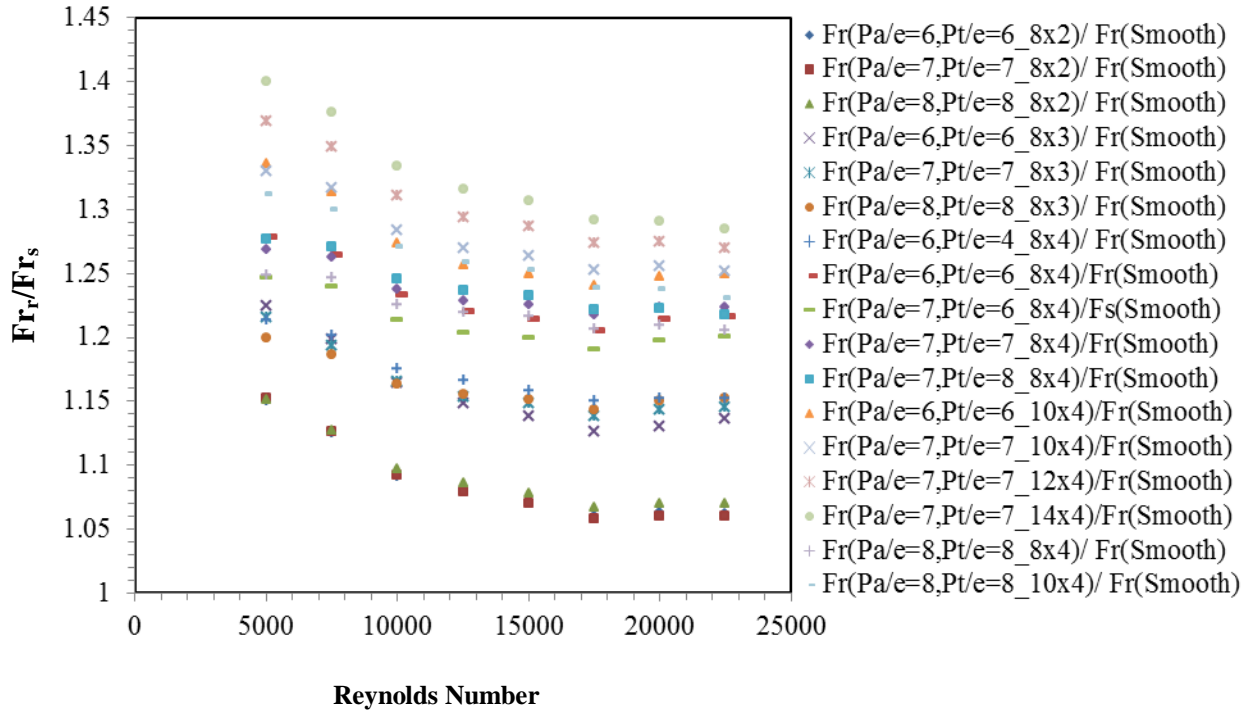


Figure 11. Variation of Friction factor ratio with respect to Reynolds number

#### 4.4. Performance parameter

The application of artificially roughened absorber plate in the duct duct of SAH increases the Nusselt number as well as the friction factor. The increase in friction in the flow region needed more pumping power so that the air can be easily driven in the SAH duct. Accordingly, in order to predict the overall performance of the SAH, a **Performance parameter** is defined as [16]

$$\text{Performance parameter, } \eta = \frac{Nu_r / Nu_s}{(f_r / f_s)^{1/3}} \quad (8)$$

The variation of the performance parameter with respected to Reynolds number for all the

studied roughness geometries is shown in Fig. 12. The Higher value of the performance parameter represents an appreciable performance of the SAH duct. It can also be observed that for entire range of Reynolds number the value of the performance parameter is greater than unity. Furthermore, for all different types of roughness geometry except  $P_d/e = 6$  and  $P_t/e = 4$  (with cross section 8x4), the value of performance parameter is highest at  $Re = 5000$ . Thereafter it decreases up to  $Re = 10000$  sharply, and then there is a slight increase from  $Re = 12500$  to 22500. The SAH gives the best performance for the roughness geometry  $P_d/e = 7$  and  $P_t/e = 7$  (with cross section 12x4).

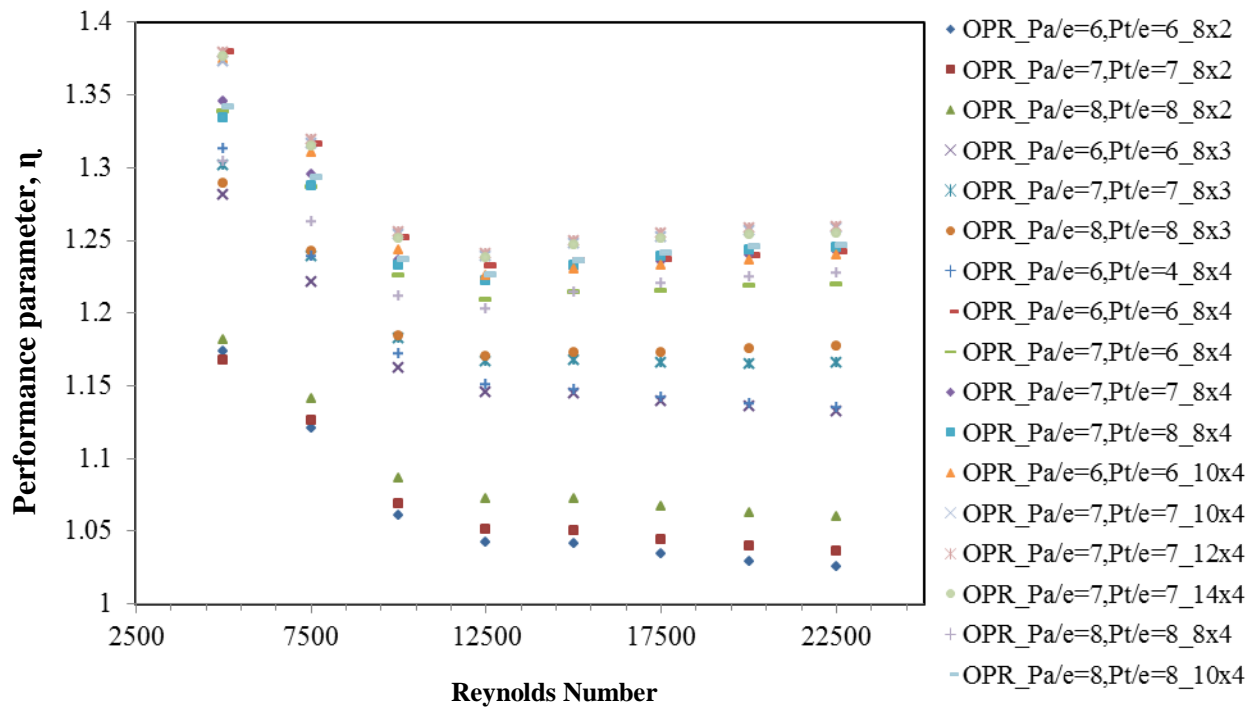


Figure 12. Variation of performance parameter with Reynolds number

## 5. Conclusions

This study presents a three-dimensional CFD analysis of the thermohydraulic performance of a rectangular duct SAH having roughened absorber plate with chamfered square roughness elements. The major findings of the study are itemized below:

1. The thermal performance of the SAH in presence of the chamfered square roughness elements is observed to be improved compare to the smooth duct. The Nusselt number increases 1.23-1.54 times for the roughened heater compared to the conventional ones for the range of Reynolds number studied.
2. Increase in Nusselt number is found with increase in Reynolds number for the roughened absorber plate. The Nusselt number of the roughened absorber plate is found in the range of 21.32 - 84.3 W/m<sup>2</sup>K and for the smooth absorber plate in range of 17.4-61.8 W/m<sup>2</sup>K.
3. Increase in friction factor is found for the roughened absorber plate with compare to that of the smooth absorber plate. The range of friction factor found is 0.0070 - 0.0149 for the roughened plate, whereas 0.0066- 0.0106 for the smooth plate.
4. The increase in Reynolds number increases the Nusselt number whereas decreases the friction factor for all sets of combination of roughness parameters.
5. The highest value of enhancement ratio of Nusselt number found is 1.54 at least Reynolds number. The enhancement ratio of Nusselt number
- 6.

7. decreases with increase in Reynolds number for all sets of configurations.

8. The highest value of friction factor ratio found is 1.4 at least Reynolds number. The friction factor ratio also decreases with increase in Reynolds number for all sets of configurations.

9. The Roughness geometry with relative roughness pitch (transverse and longitudinal) of 7, relative roughness height of 0.088 mm and 12 mm cube arm is found to have the best performance parameter.

### Nomenclature

L	Solar air heater duct length, mm
H	Solar air heater duct height, mm
W	Solar air heater duct width, mm
W/H	Aspect ratio
D	The hydraulic diameter of the duct, mm
e	Roughness height of the element, mm
A	Arm length of the roughness element, mm
e/D	Relative roughness height
Re	Reynolds number
P <sub>a</sub> /e	Relative roughness pitch in longitudinal direction, mm
P <sub>t</sub> /e	Relative roughness pitch in transverse direction, mm
Nu <sub>s</sub>	Nusselt number of smooth duct
Nu <sub>r</sub>	Nusselt number of roughened duct
Fr <sub>s</sub>	Friction factor for smooth duct
Fr <sub>r</sub>	Friction factor for roughened duct
I	Heat flux, W/m <sup>2</sup>

## References

- [1] Chabane F, Moumimi N, Benramache S. Experimental study of heat transfer and thermal performance with longitudinal fins of solar air heater. *J. Adv. Res.* 2014;5: 183-192.
- [2] Hachemi A. Thermal performance enhancement of solar air heaters, by a fan-blown absorber plate with rectangular fins. *Int. J. Energy Res.* 1995;19:567-577.
- [3] Chabane F, Moumimi N, Benramache S, Bensahal D, Belahssen O. Collector efficiency by single pass of solar air heaters with and without using fins. *Eng. J.* 2012;17:43-55.
- [4] Ibrahim Z, Ibarahim Z, Yatim B, Ruslan H Md. Thermal efficiency of single-pass solar air collector. *AIP Conference Proceedings* 1571, 90 (2013); doi: 10.1063/1.4858635.
- [5] Roy A, Hoque E Md. Performance analysis of double pass solar air heater with packed bed porous media in Rajshahi. *AIP Conference Proceedings* 1851, 020010 (2017); <https://doi.org/10.1063/1.4984639>.
- [6] Rajpoot SS, Koli DK. CFD analysis of solar air heater duct with rectangular rib surface. *Int. J. Eng. Trends Tech.* 2013;4: 3006-3011.
- [7] Dogra S. Effect of artificial roughness on thermal and thermo-hydraulic efficiency in rectangular duct of a double pass solar air heater by using transverse ribs on the absorber plate. *Int. J. Mod. Eng. Res.* 2013;3: 2271-2274.
- [8] Kumar TS, Thakur NS, Kumar A, Mittal V. Use of artificial roughness to enhance heat transfer in solar air heaters - a review. *J. Energy Southern Africa* 2010;21:35-51.
- [9] Vyas AA, Shringi D. CFD based thermal efficiency analysis of solar air heater with smooth plate and perforated plate. *Imp. J. Interdisc. Res.* 2017;3:415-422.
- [10] Tapas V, Sao AK, Sharma P. Computational analysis of an artificial roughened surface of solar air heater. *Int. J. Innovative Res. Sci. Eng. Tech.* 2015;4:12205-12212.
- [11] Prasad BN, Saini JS. Effect of artificial roughness on heat transfer and friction factor in a solar air heater. *Solar Energy* 1988;41:555-560.
- [12] Karwa R, Bairwa RD, Jain BP, Karwa N. Experimental study of the effects of rib angle and discretization on heat transfer and friction in an asymmetrically heated rectangular duct. *J. Enhanced Heat Transf.* 2005;12:343-55.
- [13] Arjumand Rasool, Adnan Qayoum. Numerical analysis of heat transfer and friction factor in two-pass channels with variable rib shapes. *International Journal of Heat and Technology.* 36 (9) 2018, 40-48. <https://doi.org/10.18280/ijht.360106>
- [14] ANSYS FLUENT 13.0 Theory Guide, ANSYS Inc., 2010.
- [15] Thakur SK, Mittal V, Thakur NS, Kumar A. Heat transfer and friction factor correlations for

rectangular solar air heater duct having 60° inclined continuous discrete rib arrangement. *British J. Appl. Sci. Tech.* 2011;1:67-93.

[16] Kumar M, Varun. A computational fluid dynamics investigation of solar air heater duct provided with inclined circular ribs as artificial roughness. *Bonfring Int. J. Ind. Eng. Manag. Sci.* 2014;4:115-120.